Article:
Elgy, I.D., Clarke, S.D., Fuller, B.J. et al. (2021) Deformation of Armox 440T plates subject to buried explosive charge detonations: A benchmark for appliqué systems. International Journal of Impact Engineering, 150. 103819. ISSN: 0734-743X

https://doi.org/10.1016/j.ijimpeng.2021.103819

Deformation of Armox 440T Plates Subject to Buried Explosive Charge Detonations: A Benchmark for Appliqué Systems

I. D. Elgy[a,*], S. D. Clarke[b], B. J. Fuller[b], A. D. Barr[b], D. W. Armstrong[a], M. T. A. Gant[a], J. J. Keirl[a], G. C. E. Porter[a], I. D. Softly[a], A. Tyas[b,c]

[a]*Dstl Porton Down, Salisbury, Wiltshire, SP4 0JQ, UK*
[b]*Department of Civil & Structural Engineering, University of Sheffield, Mappin Street, Sheffield, S1 3JD, UK*
[c]*Blastech Ltd, The Innovation Centre, 217 Portobello, Sheffeld, S1 4DP, UK*

Abstract

Loading of vehicle undercarriages from the detonation of shallow-buried explosives remains a serious threat to life in conflict and post-conflict zones. One method to protect lightly-armoured vehicles is to retrofit them with appliqué armour, which must be strong enough to provide adequate protection, but light enough to maintain vehicle manoeuvrability. A key performance metric of this armour is its deformation under loading, which must be limited to avoid impact upon vehicle occupants. The high-strength steel Armox 440T is commonly used due to its high load capacity, strength-to-weight ratio, ductility and low cost: as other protection systems are developed, it would be of great benefit to compare their deformation against an Armox 440T benchmark. However, no definitive benchmarking study has been published to date, mainly due to the difficulties in ensuring repeatable loading from complex buried detonations.

This paper presents experiments which underpin such a benchmarking study, building on the authors' previous work to establish a methodology which produces very consistent loading from shallow-buried detonations. Tests were conducted with a range of explosive masses and plate thicknesses, with target plates secured in a purpose-designed frame to produce simple, consistent boundary conditions. Plate deformations captured by stereo high-speed digital image correlation were compared to a commonly-used low-cost peak deflection method. High-speed digital image correlation was found to make highly reproducible displacement measurements with a standard deviation of 2% of the mean. The low-cost method provided slightly higher variability up to 5% of the mean value, and measurements of peak deformation were systematically 20% higher, but in

a consistent manner, with a low unit cost and without risk to expensive test equipment. The low-cost method therefore allowed the development of a multivariate regression relationship between deformation, charge size and plate thickness, which provides a benchmark for the assessment of future protection solutions.

Keywords: Vehicle Protection, Buried charges, Landmines, Plate deformation, IEDs

1. Introduction

Blast loading of armoured materials is a subject of constant study, and the variation in types of explosive charges and materials explored is necessarily vast, accounting for the uncertainty in the type, size and location of potential threats to the armour. In the protection of armoured vehicle undercarriages against ground-based threats, field trials are conducted to ascertain the potential effects of the blast on the vehicle and, importantly, the personnel it carries. Armour affected by a blast has a permanent, plastic residual deformation which is a retrospectively measurable quantity, giving some indication of the damage to the vehicle and personnel. However, the peak elasto-plastic displacement of the armour experienced during the blast is more relevant to the wellbeing of the personnel within the vehicle, as this is the main cause of compression injuries. Therefore, a reliable method for measuring and predicting the peak displacement of an armour structure from buried explosive blast loading is of paramount importance.

With its combination of high yield-stress and elongation, Armox 440T has been widely studied as a material for blast protection [1–6], but there is not yet a characterised relationship between armour plate thickness and the displacement response to blasts. The setup described in this paper lays out a modified experimental method which is relevant to military vehicles in theatre. From the recorded deflection data an equation is presented for the maximal displacement response of Armox 440T steel to buried explosive blasts from PE4 charges ranging between 400–1000 grams.

*Tel.: +44 (0) 1980 955601
Email address: idelgy@dstl.gov.uk (I. D. Elgy)

2. Background

Military vehicles are an essential part of field operations, with over 4000 of these vehicles currently in use in the UK armed forces alone [7]. These vehicles are expensive and time-consuming to design and deploy on military operations, and so adapting to ever-changing threats usually means working with a vehicle already in service, adjusting it for improved performance in the field. This can be achieved through the use of appliqués. Hence, in order to tune the defence to the threat, knowledge of the appliqué's performance is paramount.

One of the most dangerous and numerous threats to armoured military vehicles are buried explosive devices, whether traditional mines or improvised explosive devices (IEDs). These improvised devices are a widespread threat, with at least 90 countries reporting recent attacks [8]. The main objective in armouring vehicles against blasts and impacts is to ensure the minimum possible harm to personnel. In studies of active-duty personnel, up to 53% of injuries were due to IEDs [9]. In particular, the blast loading and subsequent deformation of the floor of the vehicle applies significant axial loads to the passenger, which can cause permanent and debilitating injuries to the lower leg [10], spine and neck [11]. The nature of these injuries emphasises the requirement for armour material that absorbs as much of the energy of the blast as possible, and produces the minimum peak deformation response to reduce compressional injuries.

Many studies have highlighted the effect of the geotechnical conditions surrounding a buried charge on the impulsive output delivered to a target. Geotechnical parameters, such as moisture content/saturation, air voids, bulk density, and particle size distribution, and physical parameters, such as depth of burial and stand-off distance, are known to influence the impulsive output [12–28]. Pickering et al. [22] showed that, for charges buried above a critical depth, impulse and the resulting deformation of a steel plate generally increase with increasing depth of burial. Once this critical depth is reached, the impulse continues to increase with the burial depth, but the plastic deformation of the plate then starts to linearly decrease with increased depth. Clarke et al. [24] presented the factors that affect the repeatability of buried charge testing, and highlighted the importance of keeping the test soil as uniform as possible with the water content tightly controlled, contrary to the belief that density alone is enough to predict the output of an experiment [14].

For structural applications there has also been much interest in quantifying the deformation of steel plates under the impulse imparted by bare charges [29–32], with recent improvements in technology allowing the elastic, transient response to also be captured [3, 33, 34]. Testing with buried charges is not often included in these test programmes due to the increased complexities involved, although there are notable exceptions [25, 26]. The current work adapts the methodology used previously [25], eliminating the direct measurement of impulse in favour of creating the most repeatable test conditions for armour systems. For the application of armoured material as an appliqué to existing military vehicles, a parametric study of the peak deformation of armoured steel from buried charges is essential.

This paper builds on previous research, using both mechanical and optical methods to measure the peak deformation of various thicknesses of Armox 440T steel plate exposed to a range of charge sizes. An experimental methodology is also presented which is known to deliver a repeatable distribution of impulse from a buried charge, thus defining a standardised experimental methodology for measuring the relative performance of future appliqué systems.

3. Methodology

The results of two separate test series are reported, one parametric study which measured plate deformations using aluminium crush block and one focussed study which (unsuccessfully) sought to validate heterodyned velocimetry measurements[1] against digital image correlation. Because the experimental methodology was held constant between studies, the results are comparable and the digital image correlation results can be used to provide time resolved deformation data under the same test conditions.

The experimental work was conducted by Blastech Ltd. at the University of Sheffield Blast & Impact Laboratory, Buxton, UK as part of a research project funded by the UK Defence Science and Technology Laboratory (Dstl). Armour targets, approximately half-scale models of armoured vehicle dimensions, were mounted to a custom-designed rigid reaction frame to provide a con-

[1]Heterodyned velocimetry is a non-contact method of measuring the velocity-history of a moving object. It has been used with to measure explosively driven plates [35] and was being evaluated as a possible technique for measuring the deformation of complex structures where other measurement techniques were not possible.

sistent boundary condition for plate deformation measurements. Half-scale models were used to allow a future comparison of alternative material types, such as polymer composites [36] or sandwich structures [37] and obviate some of the observed difficulties in small-scale testing of such structures [36]. The frame was constructed from large-section rectangular tubing, braced to increase stiffness as shown in Figure 1. The rigid test frame was modified from that previously described in [24] by welding additional stiffening to the underside of the frame, to allow attachment of the target interface plate.

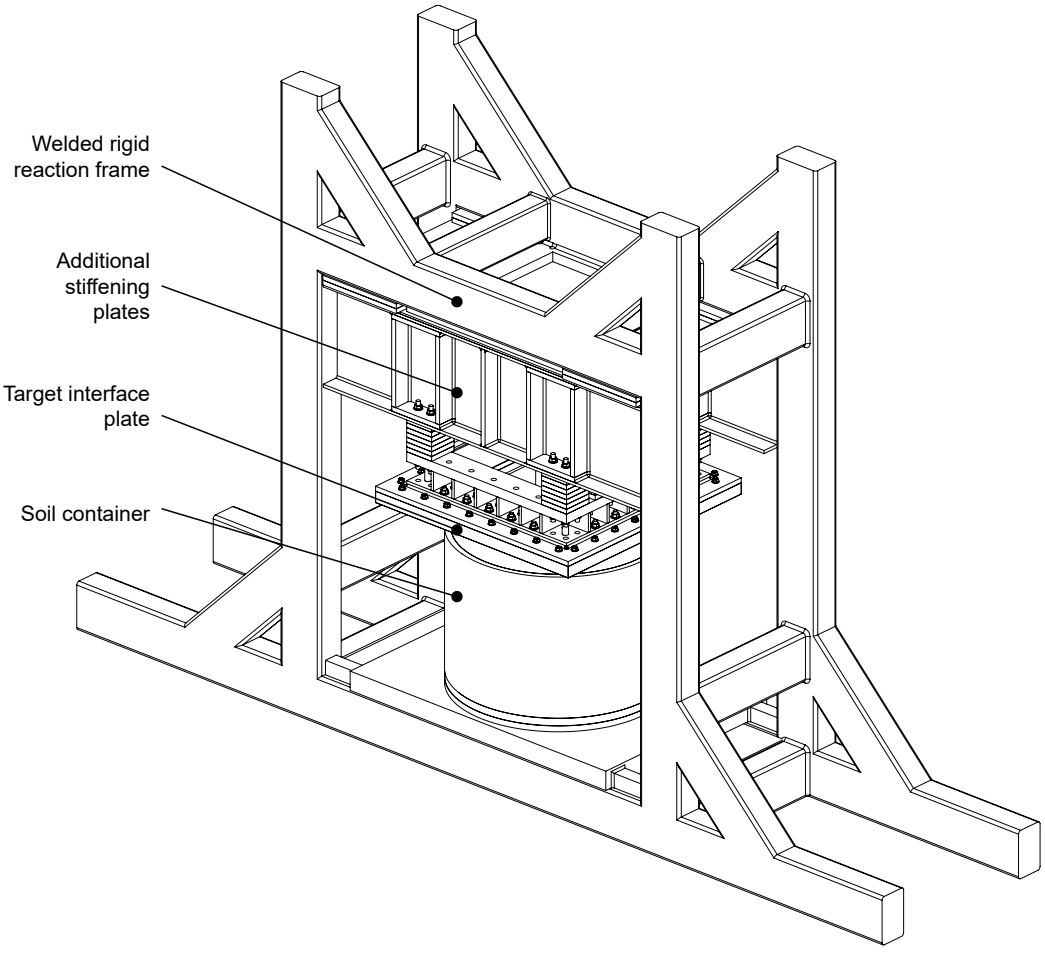

Figure 1: Overview of test apparatus

The target interface plate consisted of a fully-welded square 'picture-frame' consisting of a 1205 mm square flat plate, with the centre cut out to form a 655 mm square open aperture (Figure 2). Four trapezoidal 65 mm thick S355 steel plates were bolted to the underside of the picture

frame with M20 shoulder bolts and cap-head bolts to form a flat surface onto which to mount targets. The inside edges of the trapezoidal plates were machined to a 25 mm radius to reduce the shear-stress in the target plates [38].

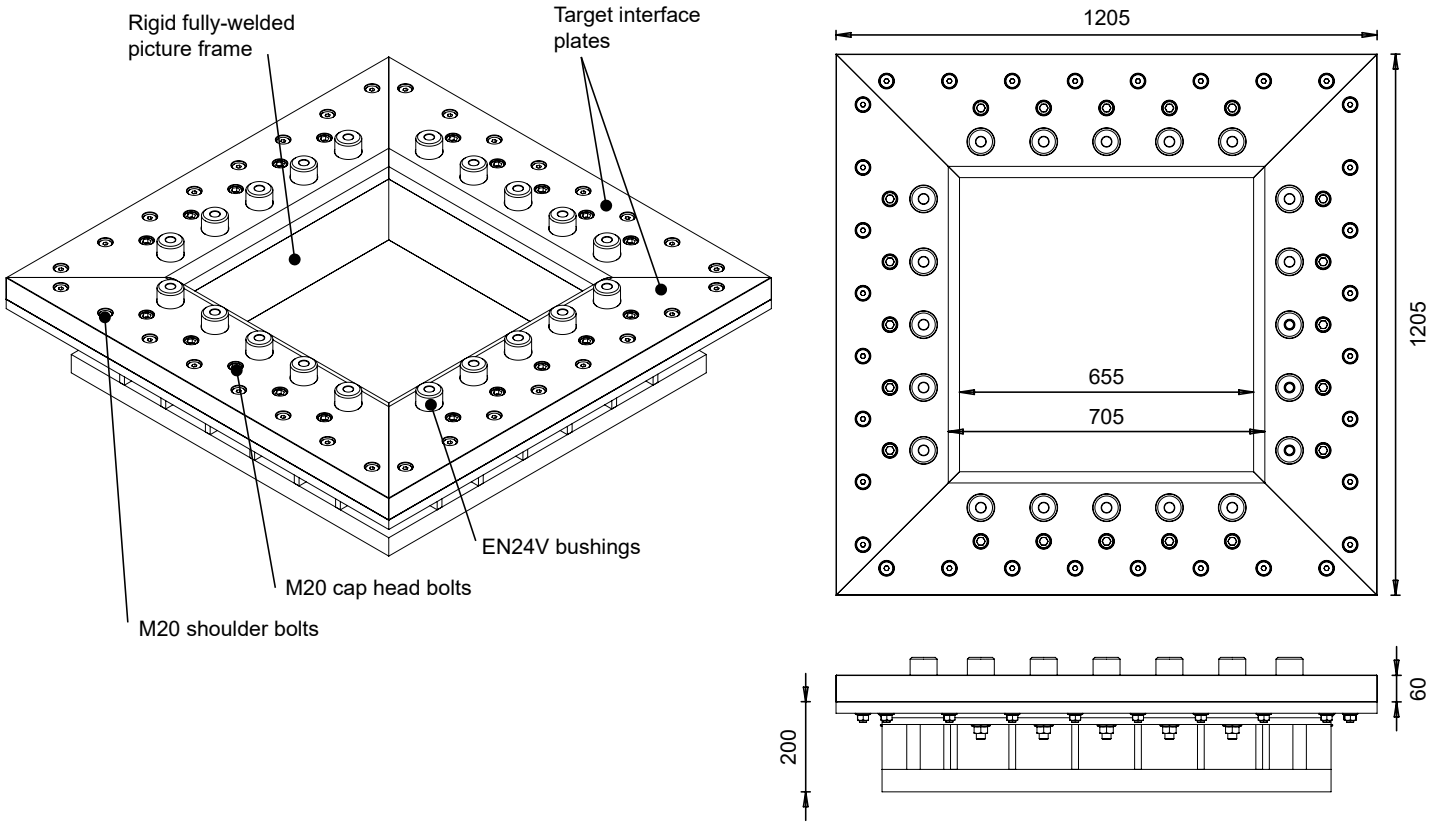

Figure 2: Schematic of the target interface plate (viewed from the underside)

Along the inside edge of each of the trapezoidal target interface plates, five 60 mm diameter EN24V bushings (twenty in total) protruded 40 mm from the underside of the flat mounting surface. These shoulder bushings fit into machined pockets in the trapezoidal plates and were therefore held captive against the lower surface of the fully welded picture frame. A 20 mm clearance hole was drilled through the centre of each bushing allowing an M20 bolt to be inserted through the hole into a captive nut on the upper surface of the picture frame as shown in Figure 3. The design of the interface plate was the culmination of an iterative design process over many years. Experiences from earlier test campaigns were that slip boundary conditions resulted in variability in deformation that was not particularly well correlated with the consistency in total impulse [25]

and this test apparatus was designed on the postulate that better control of the boundary condition would lead to more reproducible results.

Target plates consisted of 995 mm square plates of Armox 440T steel in various thicknesses representing half-scale appliqué armour; the thickness of each plate was measured with callipers prior to each test. The target plates were prepared by cutting 64 mm diameter holes into the plate to fit over the 60 mm bushings. Target plates were lifted to fit flush against the trapezoidal plates and spacers positioned around each of the bushings, of such a thickness to protrude below the lower extent of the bushing (Figure 3). A flat washer was positioned below the spacers and M20 bolts were passed through the bushings and tightened against the captive nuts. Depending on the thickness of the targets, more or fewer spacers were used to ensure the targets were held against the interface plates. By adopting this approach, the bolts holding the target to the test frame were solely in tension, while the bushings supported the shear loads from the target pulling inwards under blast loading; because of the large diameter of the bushings, the shear stress was sufficiently low to prevent plastic deformation. In this way a consistent boundary condition for the targets was ensured and the variation in target response between tests was minimised.

A 90 mm × 90 mm, 200 mm tall 5.2-1/4-25N-3003 aluminium honeycomb crush block was placed directly behind the target and braced against a rigid reaction beam, which was bolted to the test frame above the crush block. This system was used to measure the peak dynamic deflection of rear face of the target. The strength of the material is quoted as 4.3–4.6 MPa (therefore initiating crushing at a force of 35–37 kN) with a prolonged crush stress of 1.6 MPa (applying a consistent force of 13 kN) [39, 40]. To improve the positioning of the crush block, the sides of the block were wrapped in adhesive tape to provide a better adhesion when the crush block was taped to the underside of the rigid reaction beam.

3.1. Geotechnical conditions

Controlling soil parameters has been shown to effectively reduce the variability of buried charge experiments and so the methods of filling the container with soil were replicated from previous studies [24]. Soil containers were constructed from 30 mm thick rolled mild steel plate formed into a 1000 mm internal diameter, 750 mm tall cylinder, with a 50 mm thick mild steel

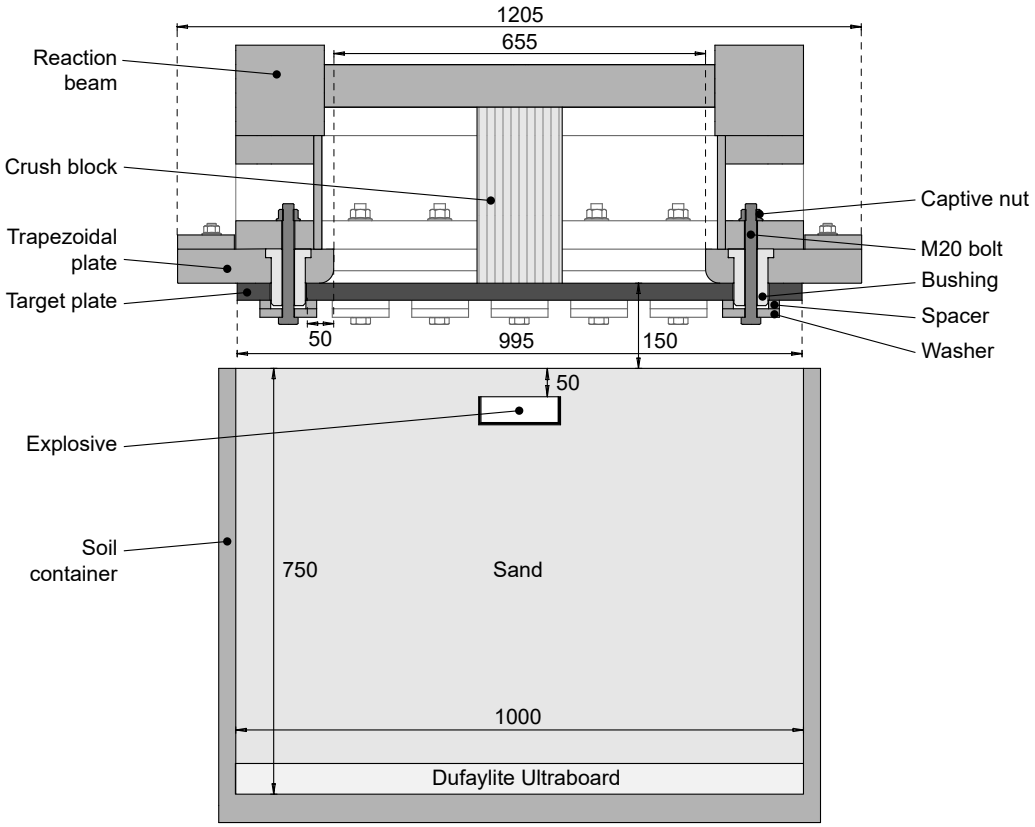

Figure 3: Sectional view through the test apparatus

plate welded to the base. A layer of cardboard energy-dissipating material was added into the base of the soil bin; three layers of 18 mm thick Dufaylite Ultraboard were cut to size and placed in the base of the soil bin and then covered with plastic sheet to protect the cardboard from moisture. The reason for this addition was to protect the base of the soil bin from plastic deformation.

The soil containers were filled with Leighton Buzzard 14/25 sand, as was used in previous studies [24]. As well as producing good levels of repeatability, explosive charges buried in this sand have been studied extensively to measure the reflected pressure imparted to flat targets [25, 41] which provides useful information for follow-on simulations.

The containers were filled in three lifts. The initial moisture content of each lift was checked prior to filling, and the mass of water required to bring the moisture content to 5±2% by mass was added to the sand. The sand was mixed in a forced action pan mixer until the water was evenly distributed. The moisture content was then re-checked and, if the moisture content was confirmed

to be within tolerance, the contents of the pan mixer were purged into the soil container, taking care to avoid sample loss. Plywood shuttering (cut to the internal diameter of the container) was placed on the surface of the soil and a stiffened steel plate (100 mm clear of the internal diameter) was seated on the timber boards. A vibrating compaction plate was placed upon the stiffened steel plate and the soil vibrated until it reached its target level of compaction based on the soil depth measured in the container. The vibrating compaction plate, stiffened steel plate and timber boards were then removed from the container with care such that the soil surface remained undisturbed. This was repeated until the container was filled. The density was then calculated based upon the internal dimensions of the soil container and mass of soil and water added. The target density for the sand was 1.62 Mg/m^3 for all tests and was achieved to within 1.45%.

3.2. Explosive setup

PE4 charges were buried in the sand. The charges were each 3:1 cylinders, packed into open-topped, 3D printed, PLA plastic cases with 4 mm thick walls and bases. The charges ranged in size from 400 g to 1000 g. During commissioning tests, the charge size was increased to induce deformation of between 50 mm and 100 mm in the targets. The lower limit was to allow measurement errors arising from surface imperfections in the deformed crush block to be small in comparison to the magnitude of the deformation measured. The upper limit was selected after observing a perforation of a target where similar plate thicknesses and charge masses were observed to undergo approximately 100 mm of deformation. Each charge was buried with an overburden of 50 mm of sand above the charge. To place the charge, a cavity was excavated which was approximately 5 mm wider than the charge geometry (depth was set precisely). Excavated material was placed into a sealed bag so that it remained at the correct moisture content. The soil containers were placed under the targets such that the stand-off distance was 150 mm for all tests, as measured from the soil surface to the rear of the target plate. By holding the distance to this plane constant, any improvements in the structural response of thicker targets must be suitably large to outweigh the increased loading experienced as a result of being closer to the detonating explosive, as would be the case for appliqué systems in operation. A non-electric detonator was inserted into the top of the explosive charge, and the soil was replaced above the charge. The mass of soil remaining

in the bag was then weighed to determine that the density of the replaced soil was the same as the excavated material. A sectional view through the test arrangement is shown in Figure 3.

3.3. Deflection measurement

Residual deflections were measured by generating 3D models of the target plates using a photogrammetric technique. For each plate 16 photographs were taken and processed into a point cloud using VisualSFM. This point cloud was then scaled to real world units in MeshLab using the length of the plate edge. Finally, MATLAB was used to mesh the point cloud to a 10 mm grid from which the position of points can be inferred. In the source photographs the average pixel represents a length of approximately 2.5 mm, and the plate edge can be identified in the point cloud within approximately 5 mm; on a 995 mm plate this corresponds to a maximum scaling error of ±1.5% on the deflection measurements. An example of the residual deflections calculated from this analysis is shown in Figure 4 for a 12 mm thick plate. The peak centre-point deflections (before the plate relaxed to the profile of the type seen in Figure 4) were measured as the distance from the deformed aluminium crush block surface to the original location of the rear target face.

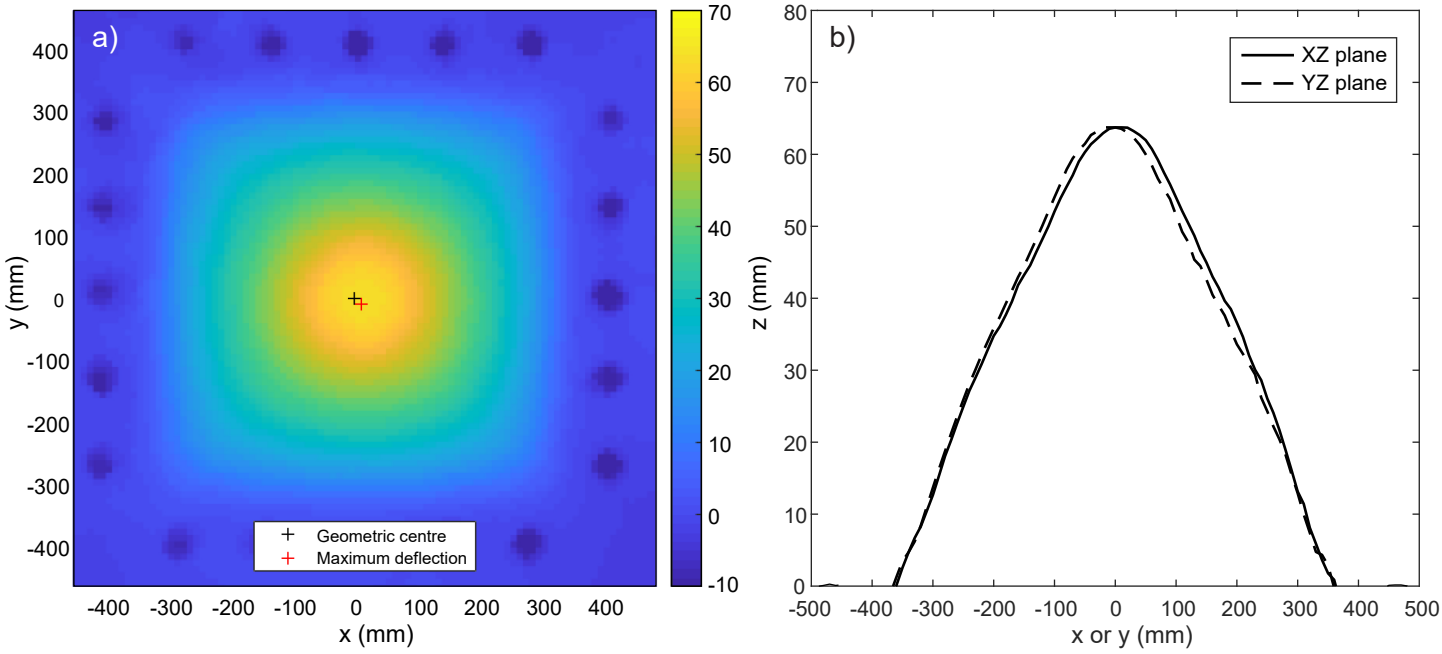

Figure 4: Example test results for a 12 mm plate against a 1000 g charge showing a) a contour plot of the deformed plate profile and b) cross-sections through the centre of the deformed profile, as measured after the test

4. Validation

One of the main advantages of using aluminium crush block for deflection measurements is its ease of deployment in aggressive environments. To gauge the absolute accuracy of the crush block system, a validation exercise was undertaken using high-speed digital image correlation (DIC) of the back face of the target plate. Due to the risk posed to the optical system from plate perforation, testing was conducted with arrangements which provided a large peak deflection but were known not to perforate the target plate. It was observed during testing that conducting DIC measurements in an outdoor environment was challenging, particularly in contrast to studies conducted indoors with much smaller test samples [42]. Video cameras had to be removed from the test apparatus at the end of each day to prevent environmental damage and the subsequent installation and recalibration reduced the number of tests which could be undertaken in any given day. Testing was impossible in wet weather conditions, owing to moisture settling on the target plate and spalling off the surface after detonation, obscuring the cameras' view. While select data points were obtained with DIC the practical considerations of testing in this way made it unfeasible to replicate the number of data points obtained with crush blocks.

Three tests were conducted with 12 mm thick Armox 440T targets against 1000 g PE4 charges. To facilitate this, the rigid reaction beam holding the crush-block was removed and a steel I-beam was inserted through the reaction frame's structure in its place. The I-beam was independently supported on concrete blocks so that it was not in contact with the reaction frame and therefore would experience lower transient accelerations during the tests. Two Photron SA-Z high speed cameras were bolted directly to the I-beam and oriented with a point 50 mm from the centre of the target plate. The angle between cameras was approximately 50° as shown schematically in Figure 5. LED lights were mounted adjacent to the cameras to provide illumination during the test.

Prior to each test, the upper face of the targets was painted with a high-contrast random pattern to facilitate DIC from the two cameras [43]. Targets were sand-blasted to remove surface corrosion and mill-scale and wiped clean. A thin layer of white paint was then sprayed onto the upper surface and allowed to dry. Black paint was then sprayed onto a piece of stainless steel wool and lightly

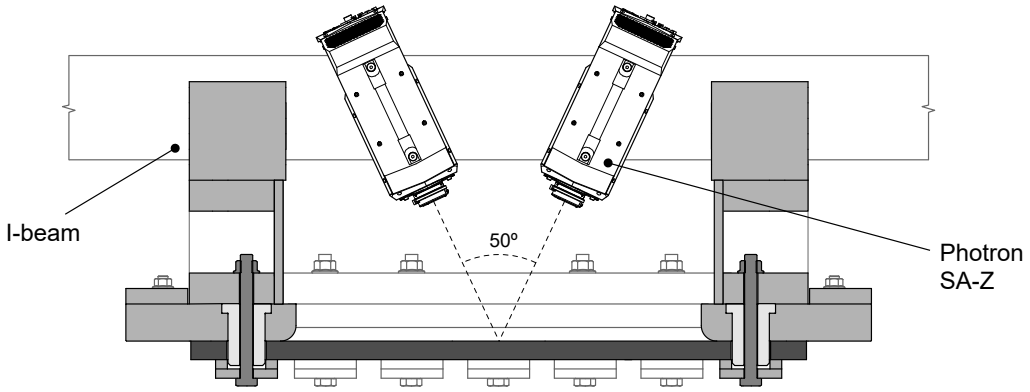

Figure 5: Experimental set-up for temporally-resolved DIC measurements

applied to the white surface to transfer a randomly-shaped patch of black paint. This process was repeated until the upper surface was approximately half covered with patches of black paint. A 30 mm diameter area at the centre of the plate was not covered with paint, and so the DIC could make no measurements in this region. (This area was used as a reflective surface during a trial of heterodyned laser velocimetry as an alternative method of displacement measurement.)

After the target plate was installed, the cameras were calibrated by placing a calibration board in the cameras' fields of view. A test image of the target plate was then recorded to confirm that the calibration had been successful and that the paint pattern's coverage was sufficient to allow the displacement field across the plate's surface to be mapped; additional black shapes were added in regions of the plate where the software could not resolve the plate's shape.

The cameras were then set to synchronised recording of the plate at 20,000 frames per second and 1,024 $\times$ 1,024 pixel resolution across the central 400 mm of the plate. They were triggered to start recording by a fibre-optic light sensor embedded in the PE4 charge, which output a TTL signal upon detonation. Typically the cameras recorded for 5 ms before entrained sand encroached around the target and obscured the cameras' views of the plates. The video footage was then processed using ARAMIS to establish the upward deformation at a range of points across the upper surface of the plate. The deformation of a point 50 mm away from the target centre (therefore within 5 mm of the footprint of the crush block position) is plotted from three tests in Figure 6, and it can be seen that the results are consistent between tests throughout the deformation. The late time DIC data also provides an additional validation for the residual deflection recorded using

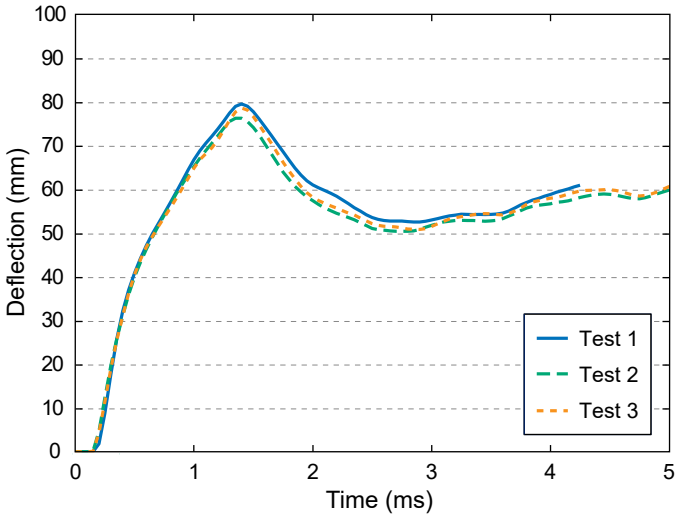

Figure 6: Upward displacement of a point 50 mm from the centre of a 12 mm thick Armox 440T plate, loaded by the detonation of a 1000 g buried PE4 charge

photogrammetry (Figure 4). From Figure 4b, the residual deflection at an offset of 50 mm from the plate centre is ≈61 mm, which agrees well with the late time deflection data in Figure 6.

Table 1: Peak displacement validation data

Method	Plate thickness (mm)		Areal density (kg/m^2)	Charge mass (g)	Peak centre-point deformation (mm) †		
	Nominal	Measured			δ	$\bar{x}$	s
DIC	12	12.4*	96.9	1000	79.5	78	1.7
		12.4*	96.9		76.3		
		12.4*	96.9		78.6		
Crush block	12	12.3	96.6	1000	95	94	1.7
		12.3	96.6		95		
		12.4	97.3		92		

Notes: *Average of all 12 mm plates tested was used (12.35 mm),
† 50 mm offset for DIC, $\bar{x}$ = mean, s = standard deviation

The peak deformation measured in each test is summarised in Table 1, and is compared against the equivalent crush block data. The precise thickness of the plates for the DIC tests was not explicitly measured, and so the plate thickness is inferred from the mean of all the 12 mm plates used in the crush blocks tests (see Table 2). The average peak deformation measured using DIC was

78 mm, with a standard deviation of 1.7 mm (2% of the mean). This standard deviation compares well with the three crush block tests with 12 mm plates and 1000 g charges, but peak deformation measurements made using the crush blocks were systematically higher than comparable tests using DIC, by an average of 16 mm. A heteroscedastic two-tailed Student's T-test returned a very low probability (0.03%) that the two test methods have the same sample mean (although with small numbers of test points this finding should be treated with caution). One reason for the discrepancy between the DIC and crush block data could be the difference in measurement locations, with the DIC measuring at an offset of 50 mm from the plate centre. Assuming the peak and residual deformed shapes are similar, it is possible to calculate that measurements at an offset of 50 mm would lead to displacement readings approximately 5 mm lower that at the true plate centre. It is also hypothesised that the initial movement of the target plate imparted momentum to the structure of the crush block, causing it to continue to compress after the plate itself had reached its maximum deformation and begun to return to its final position (as seen in Figure 6). This would mean that the crush block underwent higher levels of deformation than had actually occurred in the plate, leading to a conservative measure of peak deflection.

To investigate the credibility of this hypothesis simplified simulations were conducted using LS-Dyna. The target geometry was replicated from Figure 3 using the existing material models for the plate material [2]. A 44 mm $\times$ 32 mm, 150 mm tall crush block was added at an initial 1 mm standoff from the plate and constrained at the upper surface; while not perfectly matching the experimental geometry, this was deemed sufficiently close to investigate the phenomenon without building and meshing new components. The plate was caused to deform using the *INITIAL_IMPULSE_MINE card with a 500 g TNT 3:1 aspect ratio mine buried 72 mm deep in a 1674 kg/m^3 sand 150 mm below the target. The input parameters were manually varied until the initial velocity of the plate matched the DIC experiments to within 20%. The maximum plate deformation in the simulated case was 25% lower than the experimental case. The crush block was modelled using shell elements following an approach described by Jost el al. [44]. The honeycomb was constructed from 0.04 mm thick 5052 aluminium foil with a cell-size of 5 mm, using material models from Panicker et al. [45]. The deformation predicted in the target and lower surface of the crush-block are compared to the average experimental deformations in Figure 7. It can

be seen that, although the simulated plate deformations do not match those observed experimentally, the crush block is still predicted to continue crushing after losing contact with the target; the crush-block final deformation exceeds the maximum deformation of the target by 3 mm. Although the simulations are simplifications of the experimental setup, they show that proposed hypothesis of over-crushing in the crush-block is credible and go some way to explaining the discrepancy between crush-block and DIC results.

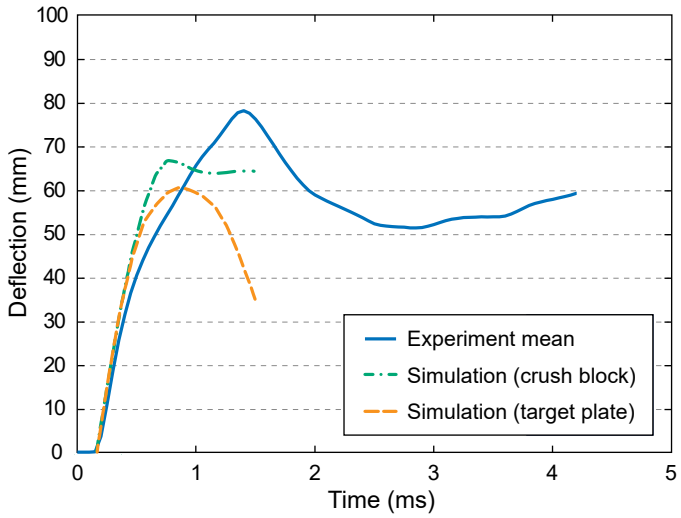

Figure 7: Average displacement of a 12 mm thick Armox 440T plate and comparative simulations of the deformation of the same plate and the consequent displacement of the lower surface of the crush block

Despite this discrepancy, the crush block data has been shown to be a repeatable measure of peak deformation, for the purposes of providing a systematic comparison between appliqué systems. Crush blocks have the additional benefits over DIC of being low-cost, quick to deploy and being easy to replace in case of target perforation.

5. Results

With the validation exercise complete, twenty four tests were conducted with crush-block peak deflection measurements using a range of charge masses and plate thicknesses, which are summarised in Table 2. The charge size was initially chosen to be 400 g and then increased until appreciable deformation of the targets was observed, but without causing target rupture or damage to the test fixture. (One target was observed to rupture: a 6.2 mm thick plate subject to the

detonation of an 800 g charge.) The areal density of each target was calculated by multiplying the measured thickness by the density of the steel which was taken as 7850 kg/m^3 [2]. Areal density was used in preference to plate thickness to allow a future assessment of materials of different densities. This approach should allow the deformation induced in, for example, an aluminium alloy plate to be measured and an assessment made of whether replacing Armox 440T armour plates in armour designs could allow deformation to be reduced while maintaining the same armour mass.

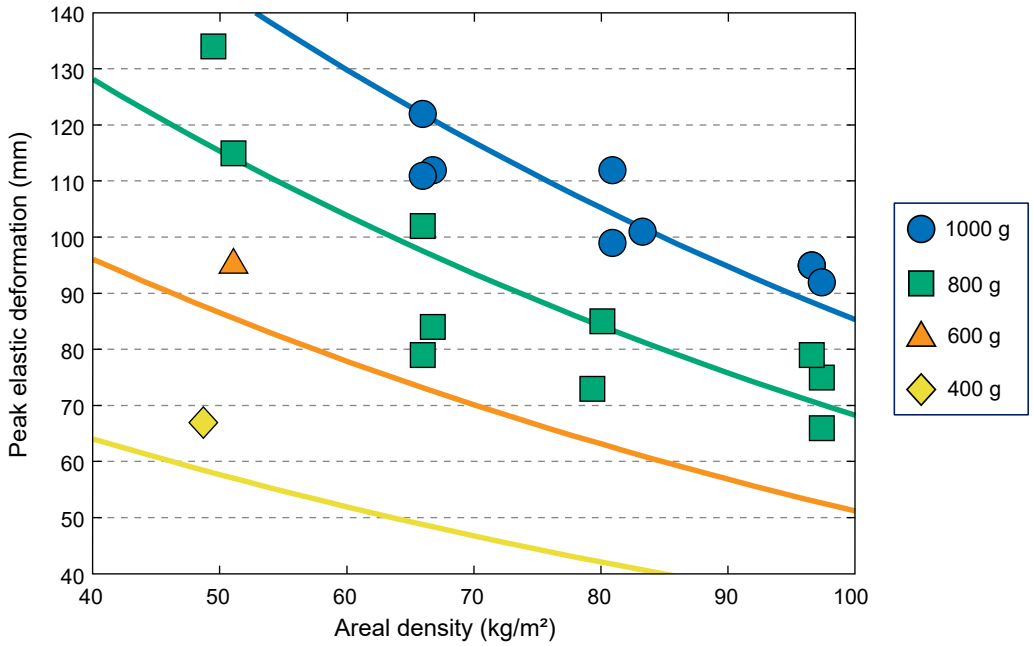

Figure 8: Peak deformation (measured from crush block compression) of Armox 440T as a function of target areal density for different explosive masses. Contours of the curve fits to the data (Equation 1) for charge masses of 400 g, 600 g, 800 g, and 1000 g have also been superimposed

The peak deformation values from Table 2 are plotted in Figure 8, where it can be seen that the peak deformation increased with explosive charge mass and decreased with areal density. It was observed that deformation levels in Figure 8 increased linearly with explosive mass (which is supported by [26]) and decreased approximately exponentially with areal density. To interpolate between data points, a single curve of the form in Equation 1 was fitted to all of the data:

$$D = aMe^{-bA} \tag{1}$$

where D is the peak deformation, M is the explosive mass and A is the areal density of the target

Table 2: Summary of peak and residual deformation results.

Plate thickness (mm)		Areal Density (kg/m^2)	Charge mass (g)	Peak centre-point deformation (mm)			Residual centre-point deformation (mm)		
Nominal	Measured			δ	$\bar{x}$	s	δ	$\bar{x}$	s
6	6.2	48.7	400	67	-	-	60	-	-
6	6.5	51.0	600	95	-	-	78	-	-
6	6.5	51.0	800	115	125	13.4	98	99	2.9
	6.2	48.7		*			97		
	6.3	49.5		134			102		
	6.2	48.7		†			†		
8	8.4	65.9	800	79	88	12.1	71	73	1.3
	8.5	66.7		84			73		
	8.4	65.9		102			74		
10	10.1	79.3	800	73	81	6.9	57	57	0.5
	10.2	80.1		85			57		
	10.2	80.1		85			58		
12	12.3	96.6	800	79	73	6.7	49	49	0.6
	12.4	97.3		66			50		
	12.4	97.3		75			49		
8	8.5	66.7	1000	112	115	6.1	93	91	4.4
	8.4	65.9		111			86		
	8.4	65.9		122			94		
10	10.6	83.2	1000	101	104	7.0	74	73	1.2
	10.3	80.9		112			72		
	10.3	80.9		99			72		
12	12.3	96.6	1000	95	94	1.7	62	63	0.9
	12.3	96.6		95			64		
	12.4	97.3		92			62		

Notes: *No data recovered, † Target rupture, $\bar{x}$ = mean, s = standard deviation

armour. The form of the function in Equation 1 was chosen such that the deformation tended to zero as explosive mass tended to zero and areal density tended to infinity; this was assessed as more likely to permit small amounts of extrapolation without yielding non-physical predictions. A multivariate least squares method was used to fit Equation 1 to the data and determine the constants a and b. An error function (E) was calculated from the 24 data points (labelled i) using Equation 2.

$$E = \sum_{i=1}^{24} (aM_i e^{-bA_i} - D_i)^2 \tag{2}$$

A Generalized Reduced Gradient non-linear solver was then used to arrive at a numerical approximation of the constants a (0.24367 mm/g) and b (0.01050 m^2/kg) which minimised the size of the error (E). Using these values, contours of M = 400 g, 600 g, 800 g and 1000 g are superimposed on the data in Figure 8.

As there are more data points at 800 g and 1000 g charge-weights, the curve-fitting algorithm preferentially fits the data at those charge masses. Consequently, the curves described by Equation 1 are a better fit to the higher charge weights than the 400 g and 600 g data points. Because Equation 1 is not linear (and cannot be readily linearised), many of the conventional methods for analysing the quality of a data fit are not appropriate and confidence intervals cannot be applied to Figure 8. An estimate of the confidence intervals, however, can be made by treating the 800 g and 1000 g data sets as independent data with constant M, linearising Equation 1 and using linear regression to apply confidence intervals to the data. This is shown in Figure 9. These confidence intervals are likely to be similar to the confidence which can be applied to the data fit shown in Figure 8.

The quality of the fit could likely be improved by modifying the form of Equation 1 but, in the absence of a physical justification for introducing additional degrees of freedom into the model, it was deemed to be sufficiently accurate to form a baseline appliqué benchmark.

The benefit of fitting a single curve to the data is that performance of a different armour can be compared to the Armox 440T baseline. If a test is performed on a new armour with areal density A, and the detonation of a charge mass, M, induces a deformation D, Equation 1 can be solved to determine the areal density of Armox 440T which would experience the same level of

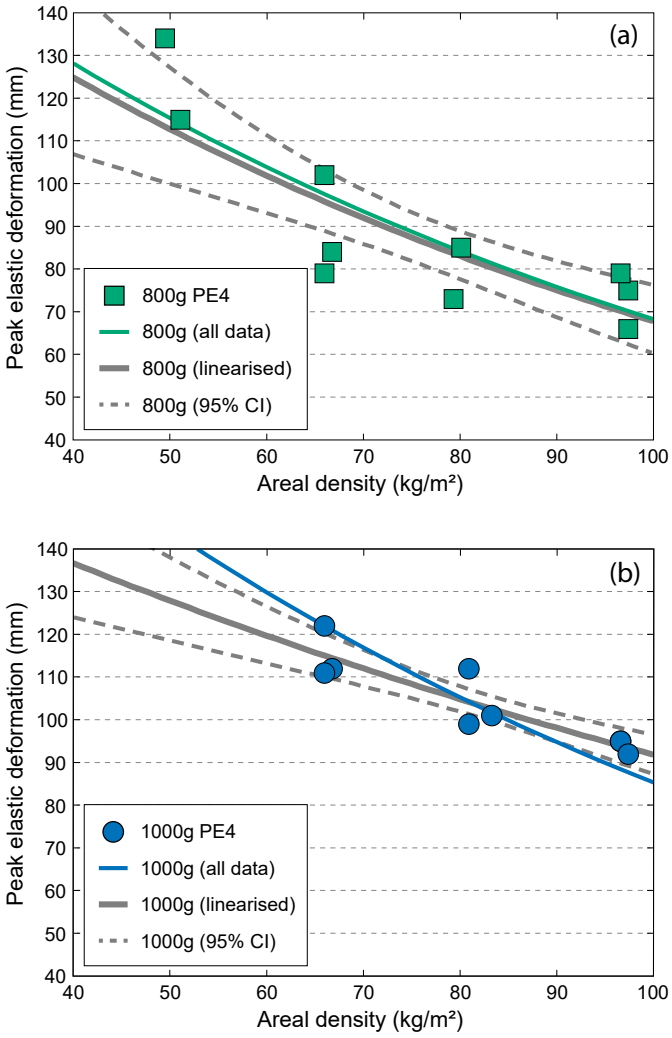

Figure 9: Peak deformation (measured from crush block compression) of Armox 440T as a function of target areal density for a) 800 g and b) 1000 g explosive masses. Regression lines from the full data fit (all data) and linearised fit with constant M (linearised) along with associated 95% confidence intervals (95% CI) have also been superimposed

deformation. In this way the level of mass saving which could be realised by the new armour can be estimated. Alternatively, Equation 1 can be solved for M to estimate to what extent the new armour will increase the protection level offered.

The residual plastic deformation showed much lower levels of variability than the peak elasto-plastic deformation (Table 2). The standard deviation on the residual deformations was 1-4 mm (1-5% of the mean value for equivalent tests), compared to the standard deviation on the peak deformations of 1-13 mm (2-14% of the mean). This implies that the measurement of residual

deformation is more reliable than the peak deformation measured using the aluminium crush block.

The residual plastic deformation is strongly correlated to peak elasto-plastic deformation (Figure 10), but does not appear highly correlated with other factors. Fitting a least-squares trend line to all the data shows a gradient of 0.77 (and a constant offset of 2 mm). As a result, the proportion by which a plate relaxes to its final, plastically deformed, state is relatively constant over the levels of deformation observed; plates appear to relax by between 15 mm and 35 mm.

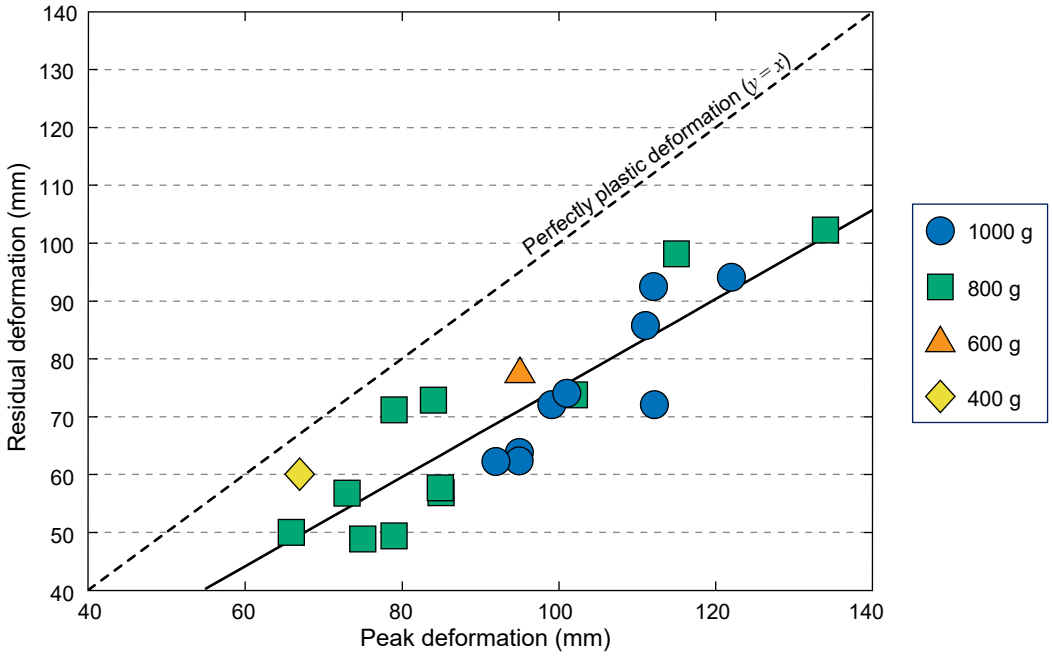

Figure 10: Residual plastic deformation of Armox 440T, as a function of peak elasto-plastic deformation for different target areal density and explosive masses, with solid black trend line

6. Summary and conclusions

Plates of Armox 440T representing half-scale models of armoured vehicle appliqué plates were tested against the loading from explosive charges buried in a uniform sand (Leighton Buzzard 14/25). A new experimental methodology has been developed to allow repeatable testing while minimising boundary effects.

A validation exercise was undertaken with a small number of tests using DIC. This showed that the peak deformation was reached within approximately 1.5 ms of detonation before the plate

relaxed to its final, plastically deformed state. Overall consistency of repeat tests using the crush block appeared to show a lower level of repeatability, implying that DIC is a more reliable way of consistently measuring the peak deformation in the target although the calibration process is more onerous which reduces the number of tests which can be conducted in a day.

The level of deformation measured appeared to depend on the method used to make the measurements. Using DIC techniques provided a less variable measurement of the peak dynamic deformation but produced measurements (in like-for-like tests) on average 16 mm (25%) lower. It is hypothesised that this arises from momentum being imparted to the crush gauge early on in the interaction which causes it to continue to compress after the deformation of the target has ceased. It may be possible to minimise this effect by using a crush block which is initially stood-off from the target plate to reduce the momentum imparted to the crush block. As a result care should be taken when conducting testing of this type to ensure that differences in armour system performance are not masked by changes in the way in which deformation is measured.

For the geotechnical conditions considered in this method, the peak deformation, D, as recorded from an aluminium honeycomb crush block, depends on the armour areal density, A, and the detonation of a charge mass, M, according to:

$$D = 0.24367 M e^{-0.0105A} \tag{3}$$

The peak deformation of Armox 440T can therefore be used as a baseline for testing other armour systems. Conducting a small number of tests of a new armour system of a given areal density allows the level of deformation to be measured. Equation 3 can then be solved to determine estimates of:

- the reduction in armour areal density (for a given charge mass) that the new armour can offer for no increase in peak deformation; and
- the increase in threat level that can be realised without increasing the armour's areal density and peak deformation.

Acknowledgements

This research was funded by CSA S&T Portfolio via the Dstl Land Systems Programme.

[1] Kartikeya, Prasad S, Bhatnagar N. Finite Element Simulation of Armor Steel used for Blast Protection. Procedia Structural Integrity. 2019;14:514–520.

[2] Mehreganian N, Fallah AS, Boiger G, Louca L. Response of Armour Steel Plates to localised Air Blast Load – A Dimensional Analysis. Int J of Multiphysics. 2017;11(4).

[3] Mehreganian N, Louca LA, Langdon GS, Curry RJ, Abdul-Karim N. The response of mild steel and armour steel plates to localised air-blast loading-comparison of numerical modelling techniques. Int J Impact Eng. 2018;115:81 – 93.

[4] Mehreganian N, Fallah AS, Louca LA. Inelastic dynamic response of square membranes subjected to localised blast loading. Int J Mechanical Sciences. 2018;148:578–595.

[5] Buchar J, Rolc S. Response of layered structures to buried charge explosion. Proceedings of 9th international conference on the mechanical and physical behaviour of materials under dynamic loading, Brussels. 2009;p. 1783–1787.

[6] Elgy ID, Pope DJ, Pickup IM. A study of combined particle and blast wave loading of structures. Journal de Physique IV. 2006;134(1):467–471.

[7] UK Ministry of Defence. UK Armed Forces Equipment and Formations. UK, National Statistics. 2018;.

[8] United Nations Security Council. Fifteenth report of the Analytical Support and Sanctions, Monitoring Team. 2014;S/2014/41.

[9] Ramasamy A, Harrison SE, Clasper JC, Stewart MP. Injuries from roadside improvised explosive devices. Trauma. 2008;65(5):910–914.

[10] Ramasamy A, Hill AM, Masouros S, Gibb I, Phillip R, Bull AM, et al. Outcomes of IED foot and ankle blast injuries. J Bone Joint Surg Am. 2013;95(5).

[11] Ragel BT, Allred CD, Brevard S, Davis RT, Frank EH. Fractures of the thoracolumbar spine sustained by soldiers in vehicles attacked by improvised explosive devices. Spine. 2009;34(22):2400–2405.

[12] Wenzel AB, Esparza ED. Measurement of pressures and impulses at close distance from explosive charges buried and in air. U.S. Army Mobility Equipment Research and Development Center, Fort Belvoir, Virginia, USA; 1972.

[13] Wenzel AB, Esparza ED. The response of armor plates to landmines using model experiments. U.S. Army Tank-Automotive Command (TACOM) Research and Development Center, Warren, Michigan, USA; 1974.

[14] Westine PS, Morris BL, Cox PA, Polch EZ. Development of Computer Program for Floor Plate Response from Land Mine Explosions. U.S. Army Tank-Automotive Command (TACOM) Research and Development Center, Warren, Michigan, USA; 1985. 13045.

[15] Hlady SL. Effect of soil parameters on landmine blast. 18th Int Sym on the Military Aspects of Blast and Shock, Bad Reichenhall, Germany. 2004;.

[16] Bergeron DM, Trembley JE. Canadian research to characterize mine blast output. In: Proceedings of the 16th international symposium on the military aspects of blast and shock, Oxford, UK; 2000. p. 501–511.

[17] Fourney WL, Leiste U, Bonenberger R, Goodings DJ. Mechanism of Loading on Plates Due to Explosive Detonation. Fragblast: the International Journal for Blasting Fragmentation. 2005;9:205–217.

[18] Anderson CE, Behner T, Weiss CE. Mine blast loading experiments. Int J Impact Eng. 2011;38(8-9):697–706.

[19] Børvik T, Olovsson L, Hanssen AG, Dharmasena KP, Hansson H, Wadley HNG. A discrete particle approach to simulate the combined effect of blast and sand impact loading of steel plates. Journal of the Mechanics and Physics of Solids. 2011;59(5):940–958.

[20] Ehrgott JQ, Rhett RG, Akers SA, Rickman DD. Design and fabrication of an impulse measurement device to quantify the blast environment from a near-surface detonation in soil. Experimental Techniques. 2011;35(3):51–62.

[21] Fox DM, Huang X, Jung D, Fourney WL, Leiste U, Lee JS. The response of small scale rigid targets to shallow buried explosive detonations. Int J Impact Eng. 2011;38(11):882–891.

[22] Pickering EG, Chung Kim Yuen S, Nurick, GN, Haw P. The response of quadrangular plates to buried charges. Int J Impact Eng. 2012;49:103–114.

[23] Fox DM, Akers SA, Leiste UH, Fourney WL, Windham JE, Lee JS, et al. The effects of air filled voids and water content on the momentum transferred from a shallow buried explosive to a rigid target. Int J Impact Eng. 2014;69:182–193.

[24] Clarke SD, Fay SD, Warren JA, Tyas A, Rigby SE, Reay JJ, et al. Geotechnical Causes for Variations in Output Measured from Shallow Buried Charges. Int J Impact Eng. 2015;86:274–283.

[25] Clarke SD, Fay SD, Warren JA, Tyas A, Rigby SE, Reay JJ, et al. Predicting the role of geotechnical parameters on the output from shallow buried explosives. Int J Impact Eng. 2017;102:117–128.

[26] Curry R. Response of plates subjected to air-blast and buried explosions [PhD thesis]. Department of Mechanical Engineering, University of Cape Town, South Africa; 2017.

[27] Denefeld V, Heider N, Holzwarth A. Measurement of the spatial specific impulse distribution due to buried high explosive charge detonation. Defence Technology. 2017;13(3):219–227.

[28] Linforth S, Tran P, Rupasinghe M, Nguyen N, Ngo T, Saleh M, et al. Unsaturated soil blast: Flying plate experiment and numerical investigations. Int J Impact Eng. 2019;125:212–228.

[29] Nurick GN, Martin JB. Deformation of thin plates subjected to impulsive loading—a review Part II: Experimental studies. International Journal of Impact Engineering. 1989;8(2):171 – 186.

[30] Neuberger A, Peles S, Rittel D. Scaling the response of circular plates subjected to large and close-range spherical explosions. Part I: Air-blast loading. Int J Impact Eng. 2007;35(5):859–873.

[31] Neuberger A, Peles S, Rittel D. Scaling the response of circular plates subjected to large and close-range spherical explosions. Part II: Buried charges. Int J Impact Eng. 2007;35(5):874–882.

[32] Chung Kim Yuen S, Nurick GN, Langdon GS, Iyer Y. Deformation of thin plates subjected to impulsive load: Part III – an update 25 years on. Int J Impact Eng. 2017;107:108 – 117.

[33] Hargather MJ, Settles GS. Laboratory-scale techniques for the measurement of a material response to an explosive blast. Int J Impact Eng. 2009;36(7):940 – 947.

[34] Curry RJ, Langdon GS. Transient response of steel plates subjected to close proximity explosive detonations in air. Int J Impact Eng. 2017;102:102 – 116.

[35] Manner VW, Pemberton SJ, Brown GW, Tappan BC, Hill LG, Preston DN, et al. Measurements of near-field blast effects using kinetic plates. J Phys Conf Ser. 2014;(500):052029.

[36] Mouritz AP. Advances in understanding the response of fibre-based polymer composites to shock waves and explosive blasts. Composites Part A: Applied Science and Manufacturing. 2019;125:105502.

[37] Birman V, Kardomateas GA. Review of current trends in research and applications of sandwich structures. Composites Part B: Engineering. 2018;142:221–240.

[38] Nurick GN, Gelman ME, Marshall NS. Tearing of blast loaded plates with clamped boundary conditions. International Journal of Impact Engineering. 1996;18(7):803 – 827.

[39] Amber Composites. AAC Amber Aluminum Commercial Honeycomb, PDS/ AAC3003/05 – Oct 10;. [Online]. Available from `https://www.jacomp.fi/wp-content/uploads/2013/07/aac3003.pdf`. [Accessed 26th October 2020].

[40] Toray Advanced Composites. Aluminum Honeycomb – Commercial Grade' AlumHC-Comm PDS v9.1 2020-01-22;. [Online]. Available from `https://www.toraytac.com/media/1af121ca-6284-4dce-8e23-50d14d56fbb4/-d2Mcg/TAC/Documents/Data_sheets/Adhesives_and_Core/Honeycomb_core/Aluminum-Honeycomb-Core-Commercial-Grade_PDS.pdf`. [Accessed 26th October 2020].

[41] Rigby SE, Fay SD, Clarke SD, Tyas A, Reay JJ, Warren JA, et al. Measuring spatial pressure distribution from explosives buried in dry Leighton Buzzard sand. Int J Impact Eng. 2016;96:89 – 104.

[42] Tiwari V, Sutton MA, McNeill SR, Xu S, Deng X, Fourney WL, et al. Application of 3D image correlation for full-field transient plate deformation measurements during blast loading. Int J Impact Eng. 2009;36(6):862 – 874.

[43] Gom technical white paper. Digital Image Correlation and Strain Computation Basics;. [Online]. Available from `https://www.gom.com/metrology-systems/aramis.html`. [Accessed 2nd January 2019].

[44] Jost T, Heubrandtner T, Ruff C, Fellner B. A New Method to Model Aluminium Honeycomb Based Crash Barriers in Lateral and Frontal Crash Load Cases. In: Conference Proceedings 7th LS-Dyna Forum; 2008. p. B–III–13–B–III–24.

[45] Panicker SS, Prasad KS, Basak S, Panda SK. Constitutive Behavior and Deep Drawability of Three Aluminum Alloys Under Different Temperatures and Deformation Speeds. Journal of Materials Engineering and Performance. 2017;26(8):3954–3969.